cogent engineering

Cogent Engineering

Taylor & Francis
Taylor & Francis Group

ISSN: (Print) 2331-1916 (Online) Journal homepage: https://www.tandfonline.com/loi/oaen20

# Electrochemical evaluation of ion substituted-hydroxyapatite on HeLa cells plasma membrane potential

**Bernard Owusu Asimeng, Elvis Kwason Tiburu, Elsie Effah Kaufmann, Lily Paemka, Claude Fiifi Hayford, Samuel Essien-Baidoo, Obed Korshie Dzikunu & Prince Atsu Anani |**

**To cite this article:** Bernard Owusu Asimeng, Elvis Kwason Tiburu, Elsie Effah Kaufmann, Lily Paemka, Claude Fiifi Hayford, Samuel Essien-Baidoo, Obed Korshie Dzikunu & Prince Atsu Anani | (2019) Electrochemical evaluation of ion substituted-hydroxyapatite on HeLa cells plasma membrane potential, Cogent Engineering, 6:1, 1614756

**To link to this article:** https://doi.org/10.1080/23311916.2019.1614756



Published online: 24 May 2019.

Asimeng et al., *Cogent Engineering* (2019), 6: 1614756
**https://doi.org/10.1080/23311916.2019.1614756**

cogent engineering

MATERIALS ENGINEERING | RESEARCH ARTICLE

# Electrochemical evaluation of ion substituted-hydroxyapatite on HeLa cells plasma membrane potential

Bernard Owusu Asimeng[1*], Elvis Kwason Tiburu[1,3], Elsie Effah Kaufmann[1], Lily Paemka[2,3], Claude Fiifi Hayford[1], Samuel Essien-Baidoo[4], Obed Korshie Dzikunu[1] and Prince Atsu Anani[1]

Received: 17 January 2019
Accepted: 30 April 2019
First Published: 06 May 2019

*Corresponding author: Bernard Owusu Asimeng, Biomedical Engineering, University of Ghana, Ghana.
E-mail: boasimeng@ug.edu.gh

Reviewing editor:
Duncan Shepherd, University of Birmingham, Birmingham, United Kingdom

Additional information is available at the end of the article

**Abstract:** This study reports the electrochemical activities of a novel ion substituted-Hydroxyapatite (HAp) material in contact with HeLa cells. The work was performed to evaluate the inhibitory effects of various concentrations of HAp on ion transfer mechanisms in HeLa cells. The materials (n = 2: HAp1 and HAp3) were prepared at different stirring times from *Achatina achatina* snail shells and phosphate-containing solution. The structure of the materials and the trace elements concentration were evaluated using x-ray diffractometry and infrared spectrometry as well as atomic absorption spectroscopy. Electrochemical studies conducted on the cells after 30 min of exposure to the materials demonstrated different responses as elucidated by cyclic voltammetry. The voltammograms revealed HAp1 to be non-redox whereas HAp3 was redox active. Minimal concentrations of HAp1 showed high anodic peak current when compared to the HeLa cells alone, indicating a hyperpolarization of the cells. The peak current gradually reduced as the concentration of HAp1 was increased, and then followed by a sudden rise suggesting inhibition of the cell action potential. HAp3 showed a wavy pattern of the anodic peak current when the material concentration was varied. Peak currents of $0.92 \pm 0.03$ nA and $0.57 \pm 0.01$ nA were recorded for HAp1 and HAp3, respectively at the highest concentration of 5 $\mu$L. The results suggest that different inhibitory mechanisms are at play on the voltage-gated ion channels of the cells, indicating the possibility of using the materials to achieve different cancer proliferation inhibition.

Bernard Owusu Asimeng

## ABOUT THE AUTHOR

Bernard Owusu Asimeng holds a BSc in Physics, MSc and PhD in Materials Science all from the Kwame Nkrumah University of Science and Technology, Kumasi, Ghana. He is a Lecturer at the Department of Biomedical Engineering, University of Ghana. His research is focused on the development of ion substituted hydroxyapatite for water treatment and therapeutic purposes. The novel material developed in this paper inhibits cancer proliferation with minimal influence on normal cells. The outcome gives the group a new direction in the study of the material for cancer treatment, locally.

## PUBLIC INTEREST STATEMENT

The conventional cancer treatment methods include the use of drugs and radiation. These treatment methods cause premature cell death which results in the release of the contents of the cell to the extracellular environment. This is known to affect surrounding tissues by causing inflammation. Cancerous cells multiply by allowing inflow of ions. Thus, preventing this mechanism will inhibit their growth without the use of drugs or radiation. This work developed charged particles that are introduced to the external environment of the cell to prevent the ion intake by cancerous cells. The research shows promising results and thus needs further studies to develop the concept.

**Subjects: Biophysics; Biomaterials & Medical Devices; Medical Technology & Engineering**

**Keywords: Cyclic voltammetry; hydroxyapatite; antiproliferation material**

## 1. Introduction

Hydroxyapatite (HAp) is an inorganic material with the chemical formula $[Ca_{10}(PO_4)_6(OH)_2]$. It is similar to the mineral component of the bone and has found much use in the tissue engineering industry owing to its biocompatible nature. It is used as a scaffold to promote bone cell migration, adhesion, and growth (Fathi, Hanifi, & Mortazavi, 2008; Sopyan, Mel, Ramesh, & Khalid, 2007). HAp possesses good adsorptive properties because of its negative and positive ion constituents. This property coupled with its biocompatibility, and controllable biodegradability has made it a preferred biomaterial for the delivery of cancer drugs to cancer sites (Uskoković & Uskoković, 2011). HAp nanoparticles, like other nanocarriers, respond to certain conditions like pH to release drugs in slow and metered doses at targeted sites (Feng, Shi, Wang, Zhang, & Cao, 2013). This reduces systemic toxicity and increases the solubility of the drug (Kundu et al., 2013; Kydd et al., 2017), a solution to major limitations in chemotherapy. In spite of the advantages of nanoparticles in drug delivery, nanocarriers face design issues which include nanoparticle loading efficiency, as well as stability of nanoparticles with the attached ligands (Kumari, Ghosh, & Biswas, 2016). Some investigations have thus been focused on using the nanoparticles as drugs and not just vehicles. Reports from various studies indicate that synthetic HAp nanoparticles, without any loaded drug, exhibit inhibitory properties on liver and lung cancer cells with lesser restraints on normal cells (Tang et al., 2013; Yuan, Liu, Qian, Wang, & Zhang, 2010; Sun et al., 2016; Han et al., 2014). The cancer cells engulf the nanoparticles through endocytosis and the nanoparticles are then adsorbed onto ribosomes, interrupting the binding of mRNA. This is reported to disrupt the protein synthesis of the cells, thus inhibiting proliferation (Tang et al., 2013).

Chemotherapy, targeted drug delivery, and the use of the nanoparticles as described above, cause cancer cell death, thus preventing uncontrolled proliferation, through necrosis (forcing the cell to undergo premature death) (Azizi et al., 2017). The cell membrane ruptures causing the organelles to stop functioning. This causes all the contents, including ions in the cytoplasm to be released out of the cell. The ions then act as free radicals and pick up other ions from the surrounding normal cells causing oxidative stress (OS) which leads to cell lysis and inflammation of the surrounding tissues (Nicolson & Settineri, 2011). Literature has reports of necrosis causing leukaemia as a result of OS from chemotherapy (Zhang, Lei, Chen, Wang, & Qian, 2018). In contrast to necrosis, apoptosis (programmed cell death) occurs routinely in normal cells during growth and ageing in homeostatic mechanism to retain cell population in tissues (Elmore, 2007). It is favourable since ions are not released into the extracellular space, thus avoiding the inflammatory response (Kannan & Jain, 2000; Azizi, Ghourchian, Yazdian, & Alizadehzeinabad, 2018). Apoptosis can be initiated via two pathways: intrinsic and extrinsic depending on the origin of the death-causing stimuli (Bortner & Cidlowski, 2014; Green & Llambi, 2015). The pathways activate caspase (proteases that trigger the cell death process) which in turn requires reduction of potassium ions in the cytoplasm. Thus, ion flow across the plasma membrane and its subsequent depolarization (influx of positive ions into cell cytoplasm) are events that characterize apoptosis. Cell fragments known as apoptotic bodies are released after apoptosis. Macrophages engulf the apoptotic bodies and remove them before the cell contents can spill into the extracellular space (Franco, Bortner, & Cidlowski, 2006).

It is reported that disrupting the plasma membrane potential of cancer cells may trigger apoptosis (Zhang, Chen, Gueydan, & Han, 2017). Generally, cell plasma membranes generate potential (membrane potential) because of the imbalance of charges between the intracellular and extracellular environment. This arises from the presence of different ion channels which allow distinct ions such as $Na^+$, $K^+$, $Ca^{2+}$ and $Cl^-$ access through the voltage-gates of the ion channels based on their specific size. Because of the difference in the number of ions within the cytoplasm and the extracellular medium, a voltage difference (electrochemical gradient) is always evolving.

A normal cell tries to balance the ion concentration across the plasma membrane to achieve a resting potential through polarization. At resting potential, the cytoplasm becomes more negative. That is, more $Na^+$ are sent outside and $K^+$ are kept inside the cytoplasm (polarization). Typically, normal cells generate stimuli through polarization, for example, during muscle contraction (Lodish, Berk Arnold, Lawrence, & Baltimore David, 2000). On the contrary, cancer cells generate stimuli through plasma membrane depolarization (more $Na^+$ are taken up by the cell and the cytoplasm becomes less negative). Depolarization generates strong stimuli that communicate faster, causing rapid proliferation (Yang & Brackenbury, 2013).

To achieve apoptosis in cancer treatment, we have prepared a novel ion substituted-HAp material to influence the ion flow across the cell plasma membrane. The material is expected to release stimuli in the form of current when a low applied voltage is subjected to it. This will disrupt the depolarized membrane potential for apoptosis instigation. As proof of concept, the material is added to HeLa cells *in-vitro*, a potentiostat of a cyclic voltammetry (CV) supplies a potential to the mixture, and the ion transfer profiles from and to the cytoplasm recorded. The profiles are then related to the cell action potential. Normal human epithelial cells (RWPE-1) were used as control.

## 2. Materials and methods

### *2.1. Materials/reagents*

*Achatina achatina* (AA) snail shells were collected from snail sellers in Ghana and identified. Ammonium phosphate dibasic (APD) was purchased from Daejung chemicals & metals, Korea. HeLa cells and RWPE-1 (America Type Cell Culture (ATCC), USA) cultured in Roswell Park Memorial Institute (RPMI) medium 1640 (Sigma-Aldrich) supplemented with 10% Fetal Bovine Serum (FBS) and Penicillin-Streptomycin (PS: 100 U/mL) (Gibco, UK) were used in the cell studies.

### *2.2. HAp preparation*

AA shells were calcined at 800ºC using the method described by Asimeng et al. (2018). HAp materials (n = 2) were prepared from 0.3 M of the calcined AA shell (CAAS) material, and 0.5 M APD solutions. A quantity of 5.9 g of APD (pH 8.12) was added to 0.15 $cm^3$ of distilled water to produce 0.5 M APD solution. 0.3 M CAAS solution was also produced by adding 5.7 g of CAAS powders to 0.15 $cm^3$ of distilled water while stirring. The APD solution was added to the CAAS drop-wise and stirred using a magnetic stirrer hot plate for 1 and 3 h, respectively at a constant temperature of 40ºC. These were labelled HAp1, and HAp3 for HAp stirred at 1 and 3 h, respectively. The materials were permitted to age for 24 h and then filtered. The filtrates were dried in an oven at a 100°C for 2 h to form HAp materials (Asimeng et al., 2018).

### *2.3. Characterization techniques*

X-ray diffractometer (PANalytical Empyrean, Netherlands), with Cu Kα radiation, λ = 1.5406 Å, was used to determine the phase compositions of the materials. The scan was in steps of 2° per min and the phases identified by comparing the material patterns to the Joint Committee on Powder Diffraction Standards (JCPDS) file. The crystallite size of HAp1 and HAp3 were determined using Debye-Scherer's equation from the extreme peaks in the range of 30–35°. Infrared (IR) Spectrometer (Spectrum Two FT-IR, Perkin Elmer) was used to examine the functional groups present in the materials. The spectra were obtained over the region of 400–4000 $cm^{-1}$ and compared to the Database of ATR-FT-IR spectra of various materials. Atomic Absorption Spectrometry (PinAAcle 900 AA Spectrometer, Perkin Elmer) of selectable spectral bandwidth 0.2, 0.7, and 2.0 nm was used to determine the concentration of trace elements in the materials.

### *2.4. Electrochemical and in-vitro cell studies with hap materials*

Cells were cultured in different T-75 culture flasks of RPMI-1640 supplemented with 10% FBS, 1% PS and kept in an incubator at 37°C and 5% $CO_2$. Cells were detached from culture flasks using trypsin and kept in suspension in culture medium. The cells were grown at 3 different times and each cultured cell gave cell density which was normalized using the inhibition rate, i given as:

$$i = 1 - \frac{treated\ cell\ viability}{untreated\ cell\ viability} \times 100$$

The mixture was centrifuged and then suspended in phosphate buffer saline (PBS: electrolyte medium for the experiment). A quantity of 5 mg of each HAp material was added to 50 $\mu$L of PBS and microcentrifuged for 60 s to form a stock solution after which varying concentrations (1–5 $\mu$L) of the supernatant were pipetted into 100 $\mu$L of each cell. The bulk mixture was incubated for 30 min at room temperature before CV and viability studies using Cheap Stat Potentiostat (IORodeo, USA) with an Ag/AgCl interdigitated electrode (DropSens, UK), and a Cellometer Mini (Nexcelom, USA), respectively. 5 $\mu$L of the bulk mixture for various concentrations of HAp1 and HAp3 containing $6.30 \times 10^6$ cell/mL were pipetted onto the electrode for CV readings. 20 $\mu$L of the bulk mixture was added to 20 $\mu$L of 0.2% trypan blue prepared in PBS (pH 7.2) after which 20 $\mu$L was then pipetted on to the counting chamber of the cellometer for cell viability.

### *2.5. Statistical analysis*

The data were reported as the means, with standard deviations as the errors. One-way ANOVA and Tukey–Kramer's procedure was used to compare the variance between data groups. The statistical significance was determined with 5% confidence level ($p < 0.05$)(Chen, Bruyneel, Clarke, Carr, & Czernuszka, 2013).

## 3. Results and discussion

### *3.1. XRD analysis*

Figure 1 shows XRD patterns for raw AA shell and CAAS materials. The raw powder material pattern in Figure 1(a) has an aragonite structure. The aragonite was calcined at 800°C to convert into calcite, since calcite is more stable and commonly used for HAp preparation (Ruiz-Agudo, Putnis, & Putnis, 2014). The calcination temperature transforms aragonite to calcite and decomposes portions into calcium oxide (Yang & Brackenbury, 2013). The pattern in Figure 1(b) shows the structure of the CAAS materials and this reveals phases of calcite and calcium hydroxide. Calcium oxide absorbs moisture from the atmosphere to form calcium hydroxide. Figure 2 shows the XRD patterns of HAp prepared from CAAS and APD. The patterns demonstrate a similar structure for HAp1 and HAp3. However, the variations in the stirring time resulted in different crystallite sizes. The crystallite size calculated for HAp1 and HAp3 were 40.86 ± 4.13 and 37.82 ± 3.48 nm, respectively.

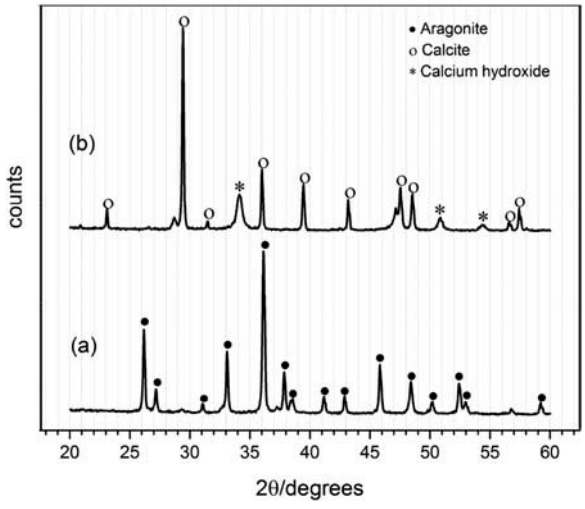


**Figure 1. XRD patterns of AA shell materials (a) raw (b) CAAS at 800°C. The raw materials show the pure phase of aragonite structure, whereas the CAAS reveals major phases of calcite and minor phases of calcium hydroxide.**

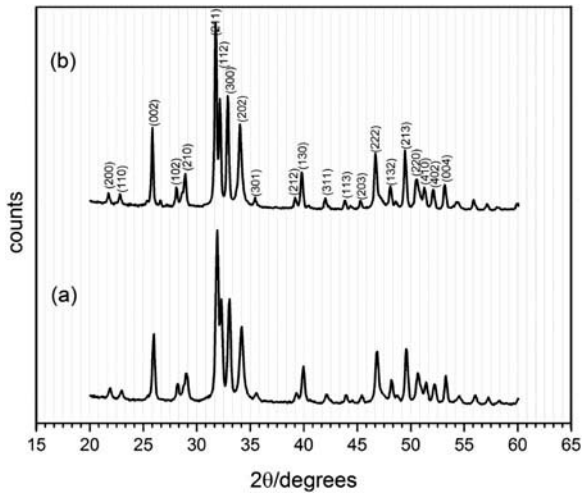


**Figure 2. XRD patterns of HAp materials prepared at varied stirring times (a) HAp1 (b) HAp3. The pattern looks similar with slight variation in the full half width maximum (FHWM).**

### *3.2. Infrared (IR) spectroscopy*

FT-IR confirms the functional groups present in the prepared materials. The fingerprints in Figure 3(a) corresponded to the aragonite structure as confirmed from the Database of ATRFT-IR spectra of various materials (Asimeng et al., 2018; Vahur, Teearu, Peets, Joosu, & Leito, 2016). The fingerprints with wavenumber 1082 $cm^{-1}$ disappeared with CAAS. The fingerprints at wavenumbers 712, 874, and 1417 $cm^{-1}$ in Figure 3(b) are those for calcite functional groups. These fingerprints support the XRD results of structural change from aragonite to calcite. The steep region around wavenumber 400 to 712 $cm^{-1}$ indicates the presence of Ca-O stretching weak bonds (Karthik, Dhanuskodi, Gobinath, Prabukumar, & Sivaramakrishnan, 2017) whereas the wavenumber at 3643 and 712 $cm^{-1}$ are the fingerprints of calcium hydroxide (Karthik et al., 2017). Figure 4 shows the fingerprints of HAp functional groups. The six phosphate groups occurred at wavenumbers 473, 563, 600, 963, 1029, and 1090 $cm^{-1}$. This indicates the symmetric vibrational modes, $\nu 1$ and $\nu 2$ of phosphate at 473 and 963 $cm^{-1}$, respectively whereas $\nu 3$ appears at wavenumbers 1029 and 1090 $cm^{-1}$. The final $\nu 4$ shows at wavenumbers 563 and 600 $cm^{-1}$. The two hydroxide groups of HAp appeared at wavenumbers 634 and 3574 $cm^{-1}$. The carbonate groups at wavenumber 874 and 1412 $cm^{-1}$ suggest that the materials are carbonated HAp. The carbonate peaks show a difference in the transmittance between HAp1 and HAp3. This variation is due to the prolonged stirring of the materials at 40◦C as reported in

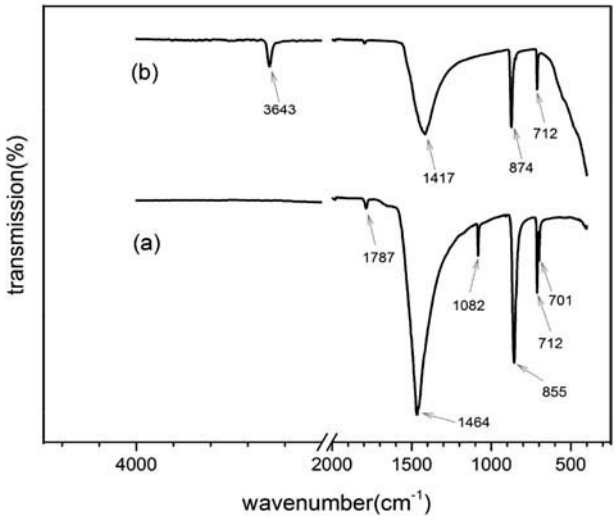


**Figure 3. FT-IR spectra (a) raw (b) CAAS materials. The raw material corresponded to aragonite structure whereas the CAAS material is made up of calcite and hydroxide groups.**

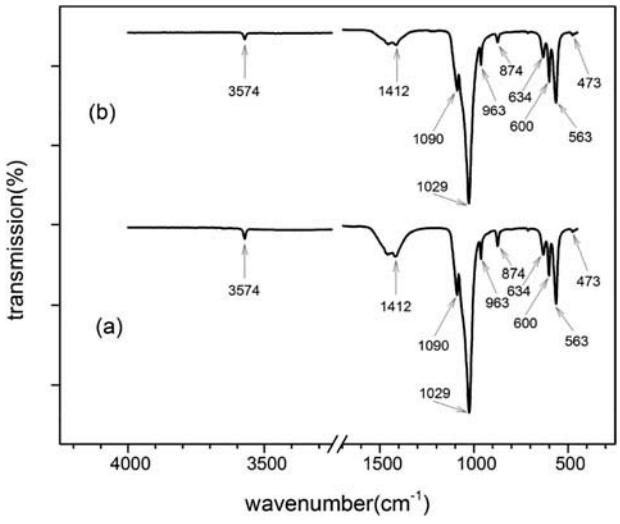


**Figure 4. FT-IR spectra of the HAp materials prepared at varied stirring times (a) HAp1 (b) HAp3. The wavenumbers at 1412 and 874 $cm^{-1}$ confirm the materials are carbonated-HAp. The differences in the carbonate fingerprints were due to the prolonged stirring temperature.**

the literature (Asimeng et al., 2018). The decomposition of the carbonate might have been the reason for the reduction of the crystallite size indicated in the XRD.

### *3.3. AAS studies*

Figure 5 shows the concentrations of trace elements in HAp1 and HAp3. The AAS studies conducted on sodium (Na), potassium (K), zinc (Zn), magnesium (Mg), lead (Pb), and cadmium (Cd) reveal higher concentrations of Na, K, and Zn ions. Mg, Pb, and Cd ions were below the detection limit of the device. The bar graphs show a considerable difference in $Na^+$ concentration in HAp1 and HAp3. The stirring times affected the concentration of $Na^+$ that were available to the surface of the electrode of the potentiostat. HAp1 has fewer $Na^+$ whereas HAp3 contains more surface ions, indicating ion substitutions in HAp1.

### *3.4. CV studies of cells with HAp materials*

Figure 6 shows the cyclic voltammograms (CV) of cell medium alone, cell medium with HeLa (cmHeLa) cells, HAp1, and HAp3. The cell medium (RPMI-1460) contains inorganic salts, and amino acids and when placed on the working electrode of the potentiostat, exhibited redox activity. The cell medium alone denoted electrons to the electrode at the oxidative half cycle and was recorded as an anodic peak current ($0.55 \pm 0.00$ nA). Conversely, when the potential

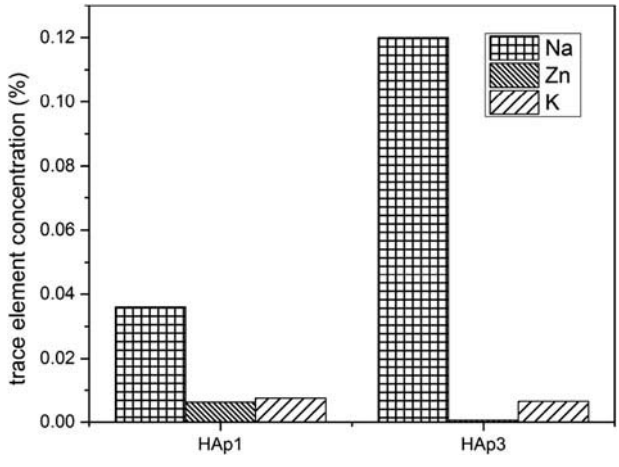


**Figure 5. AAS results of HAp1 and HAp3. Na ions were the highest trace elements present in the materials. HAp1 has fewer surface ions than HAp3, indicating that more ions were substituted in HAp1.**

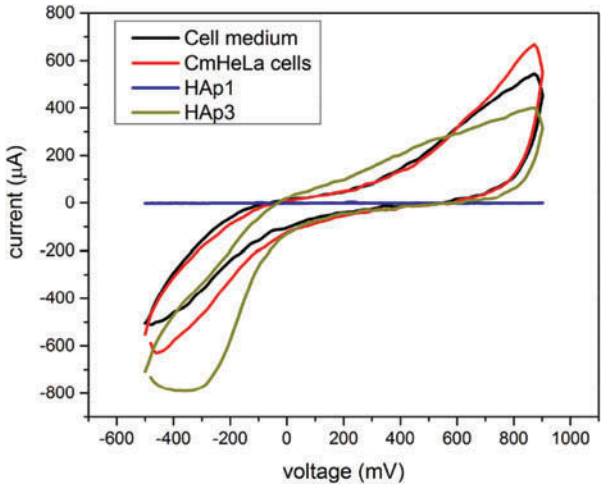


**Figure 6. Cyclic voltammograms of cell medium, cell medium with HeLa (CmHeLa) cells, HAp1, and HAp3. All the materials were exhibiting redox activity except HAp1 alone which is non-redox active.**

sweep reversed, the electrode released electrons back to the cell medium. This was recorded as a cathodic peak current on the reduction half cycle. The cmHeLa cells gave a higher anodic peak current than the cell medium alone. This result indicates that the cell released additional ions from the cytoplasm into the extracellular space (polarization), which is unusual with cancer cells. Normally, cancer cells generate depolarized membrane potential for the cell to proliferate (Yang & Brackenbury, 2013). Therefore, the recorded behaviour is due to the electrochemical gradient created by the ions present in the medium.

HAp1 and HAp3 activated in PBS solution showed non-redox and redox activities, respectively. This trend supports the AAS results where HAp1 had fewer ions on its surface than HAp3. Figure 7 shows bar graphs of anodic peak currents against HAp concentrations.

Addition of 1 µL of HAp1 into cmHeLa cells generated a higher anodic peak current compared to that of cmHeLa cells alone. Literature reports indicate that sialic acid released by the cell membrane of cancer cells promotes attachment of HAp to the cell surface, thus allowing much of the particles to be engulfed (Han, Wang, Dai, & Li, 2012). Hence, it is suspected that, the cell attaches itself to the material and results in the formation of a double-layered cell when the HAp particles are engulfed; cell membrane of the HeLa cell as one layer and the internalized HAp material as the other layer. The arrangement of

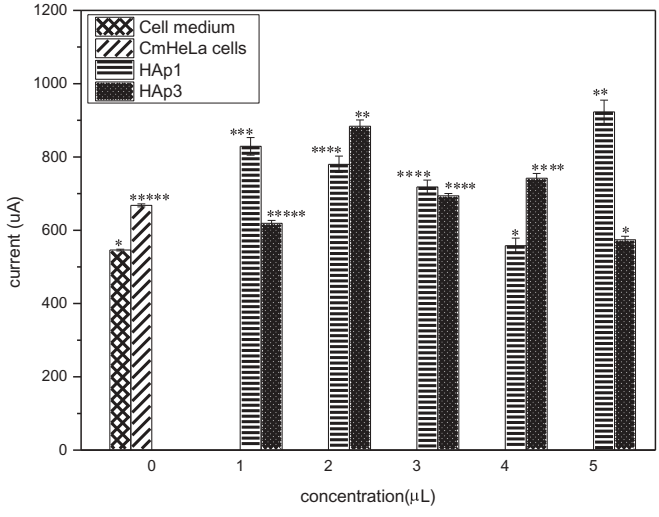


**Figure 7. The influence of HAp1 and HAp3 concentration on the anodic peak current of HeLa cells. *, **, ***, ****, and ***** represent statistical significance ($p < 0.05$) amongst groups of varied concentrations.**

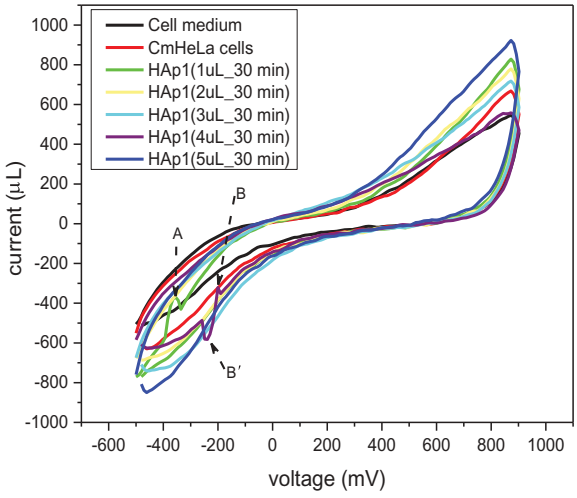


**Figure 8. Cyclic voltammograms of CmHeLa cells with different concentrations of HAp1. A and B are oxidative peaks generated due to the double layer polarization whereas B' is a reductive peak indicating electron transfer from the electrode to the available free sites.**

the double layer together with the cytoplasmic materials and the electrode of the potentiostat is believed to behave as a capacitor. Thus, upon application of voltage, a spike is observed on the cyclic voltammogram labelled A in Figure 8. The spike represents a short period of direct current (Faradic current) which acts as a stimulus to hyperpolarize the cell during the oxidation half cycle. That is, the cell's voltage-gated ion channels opened, allowing more ions to move from the cytoplasm into the extracellular medium which constitutes the higher anodic peak current recorded. As the concentration of the HAp1 material is increased, the materials formed a stack structure (as illustrated with Scheme 1) which increased the double layer thickness, d and in turn reduced the capacitance of the product formed, hence the material's Faradic current. This indicates that the concentrations of HAp1 from 2 to 4 µL did not generate stimuli to affect the cell's ion flow across the membrane, and this is evident as significantly lowering anodic peak currents as shown in Figure 7. As reported by Asimeng et al. (Asimeng et al., 2018), HAp1 has a higher adsorption capacity and so might have adsorbed some ions present in the medium to balance the membrane potential gradient creating no statistical difference between 4 µL and the medium. However, due to the reduced Faradic current, electrons are received from the electrode to balance out the charges. This is evident as a negative spike, B' in the reduction half cycle of HAp1 at 4 µL (Figure 8). As the potential sweep is reversed, the deposited electrons are released to the electrode yielding the spike B in Figure 8. At a concentration of 5 µL, the highest double layer thickness is achieved. However, the highest anodic peak current is also recorded. This is because, at this concentration, high amounts of the material is internalized and with no stimuli created to regain the membrane potential. The plasma membrane undergoes fatigue which resulted in the failure of the membrane potential. This

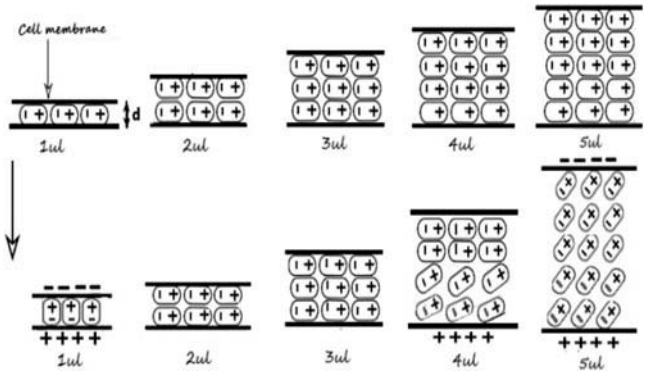


**Scheme 1. Proposed mechanistic behaviour of HAp1 on the HeLa cells. The cells form a double layer with the HAp1 material. Varying the concentration of HAp1 increases the layer thickness, d. The arrow indicates the behaviour of the layer when the potential is applied. The red signs are the electrons introduced by the electrode of the potentiostat during reduction half cycle.**

results in a high efflux of ions to the extracellular medium (hyperpolarization) hence the high peak current recorded.

Addition of HAp3 to cmHeLa cells resulted in a wavy pattern indicating a different influence on the ion transfer of the bulk mixture from that of HAp1. From Figure 7, the addition of 1 µL HAp3 caused a depolarization (inflow of ions). As shown in the AAS results (Figure 5), HAp3 has a relatively higher concentration of $Na^+$, hence leading to an inflow of ions due to the gradient established. Introducing 2 µL of HAp3 to the cells caused a hyperpolarization. The electrode recorded a higher efflux of the ions from the cells. However, further increase in the concentration of the HAp3 material does not significantly affect the membrane potential of the cells as evident in the statistical analysis (between 3 µL and 4 µL) of the recorded peak currents. Thus, 2 µL concentration of HAp3 is the critical concentration to generate hyperpolarization to disrupt the membrane potential. Cell viability test on HAp1 and HAp3 using trypan blue diazo (a dye exclusion test) confirmed a low possibility of cells to survive (Figure 9). The dye exclusion test is based on the principle that damaged cells take up permeable dyes while viable cells are impermeable to the dye. Proteins from the damaged cells interact with the dye and fluoresce for detection by the cellometer, thus quantifying them as dead cells. HAp1 and HAp3 gave cell viability of 13.44% and 14.1% at 5 µL, respectively. This supports literature reports, that altering the ion concentration in the cytoplasm greatly affects the survival of a cell (Terasaka, Kamitakahara, Yokoi, & Matsubara, 2015). The HAp3 material affected the cancerous cells to leak ions from the ion pumps as indicated in Figure 10. As a positive control, same concentrations of Hap1 and HAp3 were introduced to RWPE-1. Figure 11 shows the anodic currents at the various concentrations of the materials. Generally, lower peak currents were recorded as compared to those obtained for the cancer cells. The peak currents of HAp materials with the RWPE-1 are lower than that obtained for the RWPE-1 with the medium indicating that the materials did not hyperpolarize the membranes of the normal cells. 2015).

Studies show that the attachment of hydroxyapatite particles by normal cells is poor (Han et al., 2012). Thus, HAp materials interaction with RWPE1 showed no evidence of the formation of a capacitive product reported for HAp1 and the cancer cells (See Figure 12). There is no faradic current to stimulate polarization of the membrane. However, HAp1 adsorbed ions from the medium. The ion concentration on the surface increases and generates a concentration gradient which favoured an inflow or outflow of a few intracellular ions. The results produced a polarization proliferation signal which is needed for RWPE-1 survival. On the contrary, HAp3 has a lower adsorption capacity yet a higher concentration of surface ions (Asimeng et al., 2018). The surface ions established equal potential across the plasma membrane thus, preventing the proliferation signal. In addition, the prevention did not affect the ion pumps of the normal cells as CV in Figure

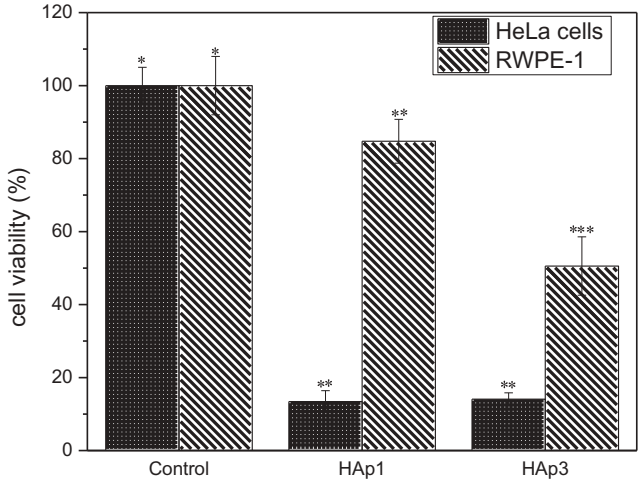


**Figure 9. Cell viability studies. HeLa cells and RWPE-1 cells were each treated with 5 µL of HAp1 or HAp3. Survival was at 84.8% and 50.6%, respectively. *, **, and *** represent statistical significance ($p < 0.05$) amongst groups.**

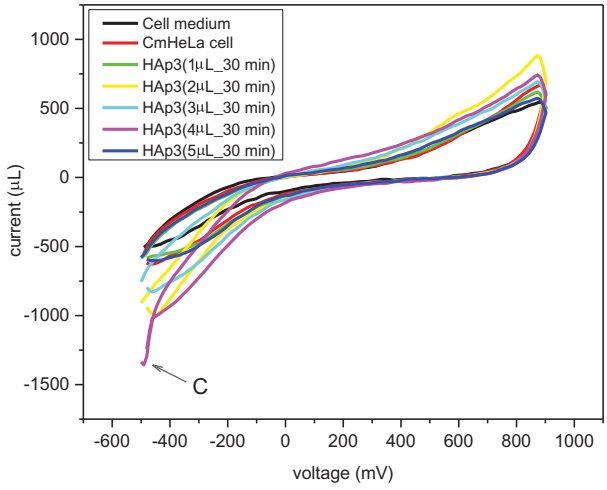


**Figure 10. Cyclic voltammograms of CmHeLa cells with different concentrations of HAp3. C indicates leakage of the $K^+$ pumps.**

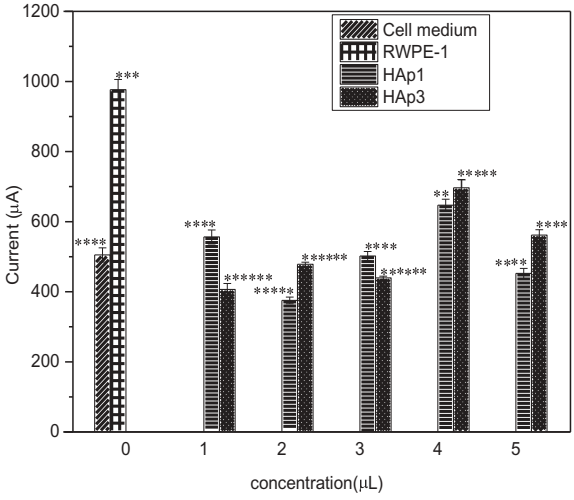


**Figure 11. The influence/impact of increasing concentration of HAp1 and HAp3 on anodic peak currents in RWPE-1 cells. *, **, ***, ****, *****, ****** and ******* represent statistical significance ($p < 0.05$) amongst groups of varied concentrations.**

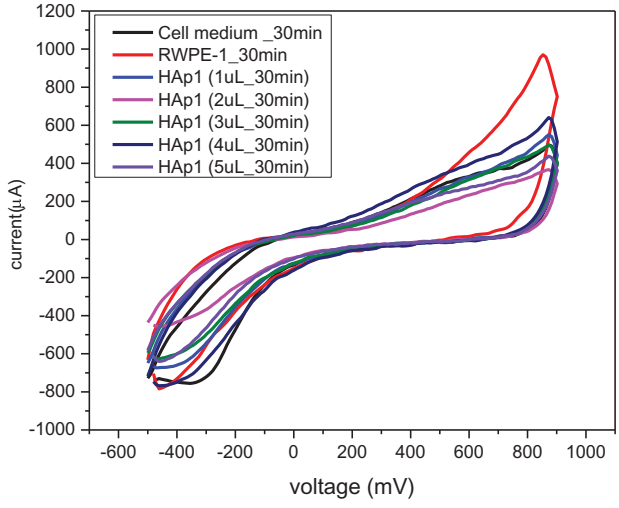


**Figure 12. Cyclic voltammograms of normal cells with different concentrations of HAp1.**

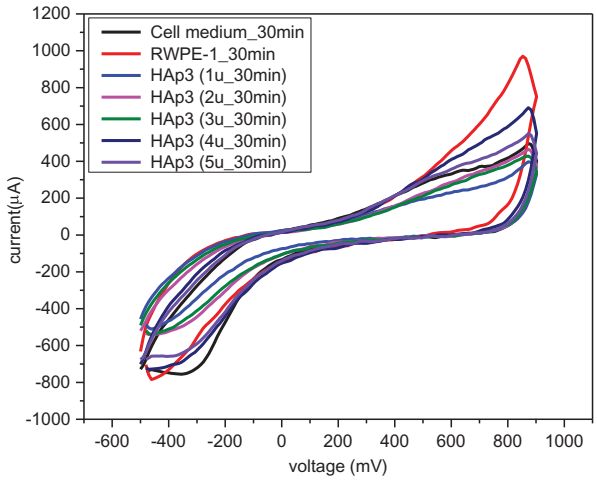


**Figure 13. Cyclic voltammograms of normal cells with different concentrations of HAp3.**

13 indicated. Cell viability studies conducted on the normal cells when exposed to HAp1 and HAp3 are indicated in Figure 9.

### *3.5. Conclusion*

Electrochemical evaluation performed on ion substituted-HAp in HeLa cells reveals that hyperpolarization of membranes of cancer cells could trigger cell death. The two materials prepared, HAp1 and HAp3, however exhibited different ion transfer mechanisms and produced a hyperpolarization of the membranes at different concentrations. HAp1 occurred at 1 µL and HAp3 at 2 µL which corresponded to anodic peak currents of $0.81 \pm 0.02$ nA and $0.90 \pm 0.02$ nA, respectively. The hyperpolarization produced was due to HAp1 forming a capacitive product with the cells and this released stimuli to affect the membrane potential gradient. HAp3 produced surface charge ions that caused a high potential gradient that released in an outflow of ions from the cytoplasm. After hyperpolarization, the cells membrane was fatigued due to the alternating cycles of polarization and depolarization and this negatively impacted cell survival. HAp1 and HAp3 recorded 13% and 14% cell viability. As a positive control, the materials were applied to normal cells (RWPE-1). The cyclic voltammograms did not show any capacitive product formation. Thus, HAp1 with RWPE-1 did not produce a hyperpolarization signal and gave high cell viability of 84%. On the contrary, the high concentration of surface ions present in HAp3 balances the potential for polarization initiation. This inhibited proliferation of the cell and thus, recorded 50% cell viability. HAp1 has the potential to be used as low voltage assisted targeted anticancer material. Further *in-vitro* studies need to be carried out to confirm the influence of HAp on the ion channels and pumps.

**Acknowledgements**
Authors acknowledge Albert Koomson, Thomas Y.A. Essel, Grace P. Cobbold for their assistance during CV studies and Mr. S. Srinivasan Balapangu cell culturing.

**Funding**
This work was supported by 'WACCBIP DELTAS grant', '[107755/7/15/Z]'.

**Author details**
Bernard Owusu Asimeng[1]
E-mail: boasimeng@ug.edu.gh
ORCID ID: http://orcid.org/0000-0002-4847-450X
Elvis Kwason Tiburu[1,3]
E-mail: tiburue@ug.edu.gh
Elsie Effah Kaufmann[1]
E-mail: eeffahkaufmann@ug.edu.gh
ORCID ID: http://orcid.org/0000-0001-7675-4333
Lily Paemka[2,3]
E-mail: lpaemka@ug.edu.gh
Claude Fiifi Hayford[1]
E-mail: chayford@ug.edu.gh
ORCID ID: http://orcid.org/0000-0002-6206-1074
Samuel Essien-Baidoo[4]
E-mail: session-baidoo@ucc.edu.gh
Obed Korshie Dzikunu[1]
E-mail: dokbiomed@gmail.com
Prince Atsu Anani[1]
E-mail: prncanani@gmail.com
[1] Department of Biomedical Engineering, University of Ghana, Legon, Ghana.
[2] West African Centre for Cell Biology of Infectious Pathogens.
[3] Department of Biochemistry, Cell and Molecular Biology, University of Ghana, Legon, Ghana.
[4] Department of Medical Lab, Tech University of Cape Coast, Cape Coast, Ghana.

**Citation information**
Cite this article as: Electrochemical evaluation of ion substituted-hydroxyapatite on HeLa cells plasma membrane potential, Bernard Owusu Asimeng, Elvis Kwason Tiburu, Elsie Effah Kaufmann, Lily Paemka, Claude Fiifi Hayford, Samuel Essien-Baidoo, Obed Korshie Dzikunu & Prince Atsu Anani, *Cogent Engineering* (2019), 6: 1614756.

**Correction**
This article was originally published with errors, which have now been corrected in the online version. Please see Correction (https://doi.org/10.1080/23311916.2019.1630795).

**Conflict of Interest**
The authors have no conflict of interest to declare.

**References**

Asimeng, B. O., Fianko, J. R., Kaufmann, E. E., Tiburu, E. K., Hayford, C. F., Anani, P. A., & Dzikunu, O. K. (2018). Preparation and characterization of hydroxyapatite from Achatina achatina snail shells: Effect of carbonate substitution and trace elements on defluoridation of water. *Journal of Asian Ceramic Societies*, *6*, 209–212.

Azizi, M., Ghourchian, H., Yazdian, F., & Alizadehzeinabad, H. (2018). Albumin coated cadmium nanoparticles as chemotherapeutic agent against MDA-MB 231 human breast cancer cell line. *Artificial Cells, Nanomedicine and Biotechnology, 46,* 787-797

Azizi, M., Ghourchian, H., Yazdian, F., Bagherifam, S., Bekhradnia, S., & Nyström, B. (2017). Anti-cancerous effect of albumin coated silver nanoparticles on MDA-MB 231 human breast cancer cell line. *Scientific Reports*, *7*, 5178.

Bortner, C. D., & Cidlowski, J. A. (2014). Ion channels and apoptosis in cancer. Philosophical transactions of the royal society of London. *Series B, Biological Sciences*, *369*, 20130104. doi:10.1098/rstb.2013.0104

Chen, Q., Bruyneel, A., Clarke, K., Carr, C., & Czernuszka, J. (2013). Collagen-based scaffolds for potential application of heart valve tissue engineering. *Journal of Tissue Science & Engineering*, *11*, 003.

Elmore, S. (2007). Apoptosis : A review of programmed cell death. *Toxicologic Pathology*, *35*, 495–516. doi:10.1080/01926230701320337

Fathi, M. H., Hanifi, A., & Mortazavi, V. (2008). Preparation and bioactivity evaluation of bone-like hydroxyapatite nanopowder. *Journal of Materials Processing Technology*, *202*, 536–542. doi:10.1016/j.jmatprotec.2007.10.004

Feng, D., Shi, J., Wang, X., Zhang, L., & Cao, S. (2013). Hollow hybrid hydroxyapatite microparticles with sustained and pH-responsive drug delivery properties. *RSC Advances*, *3*, 24975–24982. doi:10.1039/c3ra44609c

Franco, R., Bortner, C. D., & Cidlowski, J. A. (2006). Potential roles of electrogenic ion transport and plasma membrane depolarization in apoptosis. *Journal of Membrane Biology*, *209*, 43–58. doi:10.1007/s00232-005-0837-5

Green, D. R., & Llambi, F. (2015). Cell death signaling. *Cold Spring Harbor Perspectives in Biology*, *7*, a006080. doi:10.1101/cshperspect.a006080

Han, Y., Li, S., Cao, X., Yuan, L., Wang, Y., Yin, Y., … Wang, X. (2014). Different inhibitory effect and mechanism of hydroxyapatite nanoparticles on normal cells and cancer cells in vitro and in vivo. *Scientific Reports*, *4*, 7134. doi:10.1038/srep07134

Han, Y., Wang, X., Dai, H., & Li, S. (2012). Nanosize and surface charge effects of hydroxyapatite nanoparticles on red blood cell suspensions. *ACS Applied Materials & Interfaces*, *4*, 4616–4622. doi:10.1021/am300992x

Kannan, K., & Jain, S. K. (2000). Oxidative stress and apoptosis. *Pathophysiology*, *7*, 153–163. doi:10.1016/S0928-4680(00)00053-5

Karthik, K., Dhanuskodi, S., Gobinath, C., Prabukumar, S., & Sivaramakrishnan, S. (2017). Dielectric and antibacterial studies of microwave assisted calcium hydroxide nanoparticles. *Journal of Materials Science: Materials in Electronics*, *28*, 16509–16518.

Kumari, P., Ghosh, B., & Biswas, S. (2016). Nanocarriers for cancer-targeted drug delivery. *Journal of Drug Targeting*, *24*, 179–191. doi:10.3109/1061186X.2015.1051049

Kundu, B., Ghosh, D., Sinha, M. K., Sen, P. S., Balla, V. K., Das, N., & Basu, D. (2013). Doxorubicin-intercalated nano-hydroxyapatite drug-delivery system for liver cancer: An animal model. *Ceramics International*, *39*, 9557–9566. doi:10.1016/j.ceramint.2013.05.074

Kydd, J., Jadia, R., Velpurisiva, P., Gad, A., Paliwal, S., & Rai, P. (2017). Targeting strategies for the combination treatment of cancer using drug delivery systems. *Pharmaceutics*, *9*, 46.

Lodish, H., Berk Arnold, Z. S., Lawrence, M. P., & Baltimore David, D. J. (2000). Muscle: A specialized contractile machine. In *Molecular cell biology* (4th ed.). WH Freeman.

Nicolson, G. L., & Settineri, R. (2011). Lipid replacement therapy: a functional food approach with new formulations for reducing cellular oxidative damage, cancer-associated fatigue and the adverse effects of cancer therapy. *Functional Foods in Health and Disease*, *1*, 135–160.

Ruiz-Agudo, E., Putnis, C. V., & Putnis, A. (2014). Coupled dissolution and precipitation at mineral-fluid interfaces. *Chemical Geology*, *383*, 132–146. doi:10.1016/j.chemgeo.2014.06.007

Sopyan, I., Mel, M., Ramesh, S., & Khalid, K. A. (2007). Porous hydroxyapatite for artificial bone applications. *Science and Technology of Advanced Materials*, *8*, 116–123. doi:10.1016/j.stam.2006.11.017

Sun, Y., Chen, Y., Ma, X., Yuan, Y., Liu, C., Kohn, J., & Qian, J. (2016). Mitochondria-targeted hydroxyapatite nanoparticles for selective growth inhibition of lung cancer in vitro and in vivo. *ACS Applied Materials & Interfaces*, *8*, 25680–25690. doi:10.1021/acsami.6b06094

Tang, W., Yuan, Y., Liu, C., Wu, Y., Lu, X., & Qian, J. (2013). Differential cytotoxicity and particle action of hydroxyapatite nanoparticles in human cancer cells. *Nanomedicine*, *9*, 397–412. doi:10.1016/j.nano.2013.04.010

Terasaka, S., Kamitakahara, M., Yokoi, T., & Matsubara, H. (2015). Ability of hydroxyapatite synthesized from waste oyster shells to remove fluoride ions. *Materials Transactions*, *56*, 1509–1512. doi:10.2320/matertrans.M2015149

Uskoković, V., & Uskoković, D. P. (2011). Nanosized hydroxyapatite and other calcium phosphates: Chemistry of formation and application as drug and gene delivery agents. *Journal of Biomedical Materials Research - Part B Applied Biomaterials*, *96*, B: 152–191.

Vahur, S., Teearu, A., Peets, P., Joosu, L., & Leito, I. (2016). ATR-FT-IR spectral collection of conservation

materials in the extended region of 4000-80 cm−1. *Analytical and Bioanalytical Chemistry*, *408*, 3373–3379. doi:10.1007/s00216-016-9411-5

Yang, M., & Brackenbury, W. J. (2013). Membrane potential and cancer progression. *Frontiers in Physiology*, 4, 185. doi:10.3389/fphys.2013.00185

Yuan, Y., Liu, C., Qian, J., Wang, J., & Zhang, Y. (2010). Size-mediated cytotoxicity and apoptosis of hydroxyapatite nanoparticles in human hepatoma HepG2 cells. *Biomaterials*, *31*, 730–740. doi:10.1016/j.biomaterials.2010.01.042

Zhang, J. I. N., Lei, W. E. N., Chen, X., Wang, S., & Qian, W. (2018). Oxidative stress response induced by chemotherapy in leukemia treatment (Review). *Molecular and Clinical Oncology*, *8*, 391–399.

Zhang, Y., Chen, X., Gueydan, C., & Han, J. (2017). Plasma membrane changes during programmed cell deaths. *Nature Publishing Group*, *28*, 9–21.



***Cogent Engineering*** **(ISSN: 2331-1916) is published by Cogent OA, part of Taylor & Francis Group.**

**Publishing with Cogent OA ensures:**

- Immediate, universal access to your article on publication
- High visibility and discoverability via the Cogent OA website as well as Taylor & Francis Online
- Download and citation statistics for your article
- Rapid online publication
- Input from, and dialog with, expert editors and editorial boards
- Retention of full copyright of your article
- Guaranteed legacy preservation of your article
- Discounts and waivers for authors in developing regions

**Submit your manuscript to a Cogent OA journal at www.CogentOA.com**